Bond-Dependent Thole Model for Polarizability and Spectroscopy

Mark DelloStritto,[†,‡] Michael L. Klein,[†,¶,‡] and Eric Borguet[*,†,‡]

†*Department of Chemistry*

‡*Center for the Complex Materials*

¶*Institute for Computational Molecular Science, Temple University, Philadelphia, Pennsylvania 19122, United States*

E-mail: eborguet@temple.edu

Abstract

We present a new model for the calculation of molecular polarizabilities from effective atomic polarizabilities. This model is based on the Thole modified dipole interaction model for molecular polarizabilities, where the total polarizability is computed as a sum of effective atomic polarizabilities modified by dipole-dipole interactions. We extend this model by making the atomic polarizabilities explicit functions of the interatomic distances, scaling them by the radius of the volume an atom occupies in a molecule. We use the SCAN functional to show that this model, denoted TholeL, yields accurate molecular polarizabilities with little dependence on the training set. We also demonstrate that the TholeL model yields accurate polarizabilities for configurations far from the ground state structure for a wide range of molecules. Finally, we show that the TholeL model can be used to generate accurate Raman spectra for water, crystalline urea, and urea in water from ab-initio molecular dynamics simulations.

Introduction

The calculation of atomic and molecular polarizabilities is an essential component of a wide range of theoretical models and is necessary for the calculation of an equally wide range of experimental observables. In the field of molecular dynamics, it has long been recognized that static charges do not adequately model the fluctuating electric field in and around molecules, and so various polarizable force fields have been introduced. These force fields can range from simple additive models[1] to Drude oscillators[2] to Gaussian-smeared atomic charges,[3] and these models have generally been shown to improve both the electrostatic properties and equilibrium structures over non-polarizable force fields.[4] The polarizability is also key in devising QM/MM strategies for extending the range of applicability of ab-initio methods.[5] Finally, the polarizability is important for predicting optical vibrational spectra, including both Raman scattering[6] and sum frequency generation.[7,8]

While there are well-established ab-initio methods for calculating the polarizability at high accuracy, in most cases these approaches prohibitively expensive. Although it is relatively simple to calculate the polarizability from analytic derivatives of the Hamiltonian, accurate values of the polarizability often require very large basis sets.[9] It is not uncommon to require triple or quadruple zeta basis sets to obtain accurate results, and even then polarization and diffuse functions are often necessary for the polarizability to converge.[10] Not only do these basis sets require more computation time, but the addition of diffuse functions can complicate convergence, necessitating more robust and more expensive optimization algorithms. Finally, in many cases density functional theory (DFT) is the common choice for moderately sized molecules, but problems with describing electron correlation make DFT impractical for polarizability calculations.[11] Thus, one must at least use DFT with some exact exchange added, further adding to the cost of the calculation.

Owing to the prohibitive cost of polarizability calculations, there is a long history of approximate models of the molecular polarizability. Although much use has been made of bond models, atomic models of the polarizability tend to be more flexible and thereby

more common. The earliest atomic models involved simply summing over parameterized atomic polarizabilities and, despite the simplicity of such an approach, these models tend to reproduce the average polarizability quite well.[12] Such models are not very flexible, however, with parameters depending upon both the local bonding environment and the size and composition of the training set.[13] In order to ensure accuracy and general applicability, large training sets with very accurate molecular geometries are required.

The accuracy and generality of polarizability models was improved significantly with the introduction of dipole interactions. The atom dipole interaction (ADI) model for the polarizability was first introduced by Silberstein,[14] and was later refined by Applequist, Carl, and Fung.[15] These authors recognized that they could obtain polarizabilities which are self-consistent with intra-molecular electric fields by including the dipole interaction tensor into their polarizability calculations. While this method was mildly successful, it required very small atomic polarizability parameters due to the divergence of the dipole-dipole interaction at small distances. This model was significantly improved by Thole,[16] who removed this divergence by replacing the point dipoles at each atom with smeared out charge densities. The Thole model has seen widespread use in molecular simulation,[3] has been shown to maintain accuracy for large data sets,[17] has been expanded to hyperpolarizability calculations,[18] and has been extended to include both dipole interactions from both Slater-like and Gaussian-like charge densities.[19,20]

Despite the success of the ADI model, such models are generally limited to studying molecules at their ground-state geometries. The dependence of molecular polarizability on atomic position in ADI models arises from the change in the total charge density contributing to the dipole-dipole interaction with changes in bond length and angle. As the bond length in increases, more of the model charge density around a given atom is included in the dipole-dipole interaction tensor, and so the dipole interaction and the effective polarizabilities increase. While this leads to qualitatively correct dependence of the polarizability on molecular geometry, the gradient of the polarizability with respect to atomic positions

is often underestimated. This can often result in problems, including dependence on the details of the training set and difficulty predicting the relative weights of vibrational spectra. While ADI models can be used for vibrational spectroscopy,[21] they are generally restricted to narrow frequency ranges and relatively homogeneous systems where all vibrational chromophores have similar frequencies and polarizabilities.

In this work, we improve upon the ADI model by introducing atomic radius-dependent polarizabilities which reproduce the dependence of the molecular polarizability on atomic configurations. One of the reasons that a simple, additive model for the polarizability can work so well is that, in atomic units, the polarizability has units of a_0^3. The polarizability of a molecule should then be proportional to the size of the molecule, and thus in turn it should be proportional to the number of atoms in the molecule. We can take advantage of this same scaling of the polarizability to improve upon ADI models by making the atomic polarizabilities depend on the radius of the spherical "volume" occupied by the atom in the molecule. While the dependence of the polarizability on molecular geometry is a complex function of the changing hybridization of the molecular orbitals, it is useful to think of the atomic charge densities simply being stretched or compressed to occupy large or smaller spherical volumes, respectively, in the deformed molecule. The atomic polarizability will then scale correspondingly with the volume, growing and shrinking with changes in the atomic volume. In practice however, we find that the polarizability should scale with the radius of the atomic volume in order to best reproduce the molecular polarizability. Despite the simplicity of such an approach, we show that this picture allows us to accurately predict the polarizability of a wide range of molecules up to the dissociation limit.

We train this model, denoted TholeL for bond-length-dependent Thole model, on the TABS database[22] and find that it can accurately reproduce the ab-initio polarizability. We show that this model yields accurate polarizabilities not only for molecules at the ground state, but also for molecular geometries far from equilibrium. Finally, with an accurate model of the polarizability as a function of the molecular geometry over such a wide range,

we show that it is possible to efficiently calculate Raman spectra from ab-initio trajectories for a wide range of systems.

Theory

While the details of ADI models are described elsewhere, we summarize the general approach in order to introduce the expansion to volume-dependent polarizabilities. The starting point for all ADI models is the equation for the self-consistent dipole in a system of atoms interacting under the dipole approximation:

$$\mu_i = \alpha_i(E_i + T_{ij}\mu_j) \tag{1}$$

where μ_i and α_i are the dipole moments and polarizabilities of the ith atom, E_i is the external field at the ith atom, T_{ij} is the dipole interaction tensor which gives the electric field at the ith atom due to the jth atom. Note that we use Einstein notation, such that all repeated indices are implicitly summed. By inverting the above equation one obtains:

$$\alpha_i^{-1}\mu_i - T_{ij}\mu_j = E_i \tag{2}$$

Note that this can be written as a matix equation: $A\mu = E$, where the matrix A has then form of an inverse polarizability. We can thus define an *effective* polarizability α_i^{eff} as:

$$\alpha_i^{eff} = \sum_j (A^{-1})_{ij} \tag{3}$$

In Thole's initial approach, the dipole interaction tensor was calculated from a single H-atom-like charge density.[16] Since the charge density, and thereby the dipole interaction tensor, is determined by a single exponential function, we denote this as the "expontential" or "Exp" interaction. The dipole interaction tensor is then:

$$
\begin{aligned}
T_{ij} =& 3r_{ij}r_{ij}^T/r_{ij}^5\big[1-(\frac{1}{6}b_{ij}^3+\frac{1}{2}b_{ij}^2+b_{ij}+1)e^{-b_{ij}^2}\big] \\
&- Ir_{ij}^T r_{ij}/r_{ij}^3\big[1-(\frac{1}{2}b_{ij}^2+b_{ij}+1)e^{-b_{ij}^2}\big]
\end{aligned}
\tag{4}
$$

where $r_{ij} \equiv r_i - r_j$, r_{ij}^T is the transpose of r_{ij}, and I is the identity matrix. Here, $b_{ij} \equiv a r_{ij}(\alpha_i\alpha_j)^{1/6}$ is a scaling factor and a is a free parameter determined by fitting to ab-initio data.

In this work we also use a dipole interaction tensor based on the interaction between two Gaussian charge densities:[23]

$$
T_{ij} = \frac{(3r_{ij}r_{ij}^T - Ir_{ij}^T r_{ij})}{|r_{ij}|^5}\left[\mathrm{erf}(|r_{ij}|/R_{ij}) - \frac{2}{\pi}e^{-(|r_{ij}|/R_{ij})^2}\right] - \frac{4}{\sqrt{\pi}R_{ij}^3}e^{-(|r_{ij}|/R_{ij})^2}\frac{r_{ij}r_{ij}^T}{|r_{ij}|^2} \tag{5}
$$

In this case, the scaling factor R_{ij} is defined by effective atomic radii: $R_{ij} \equiv \sqrt{R_i^2 + R_j^2}$, where R_i is a radius defined by:.

$$
R_i \equiv \left(\frac{2}{3\sqrt{\pi}}\alpha_i\right)^{1/3} \tag{6}
$$

Since the interacting Gaussian charges give rise to an term with an error function, we denote equation 5 as the "Erf" dipole interaction. The atomic radius is defined in terms of the atomic polarizability by taking the limit $r_{ij} \to 0$, leaving a constant term:[24] $4/(3\sqrt{\pi})R_{ij}^{-3}$. We interpret this constant term as twice the self-energy of a single dipole, since the interaction as $r_{ij} \to 0$ gives the interaction between two dipoles at zero distance. Since the interacting Gaussian charges give rise to a term with an error function, we denote equation 5 as the "Erf" dipole interaction.

In most approaches the initial polarizabilities α_i are parameters determined from a fitting procedure to large set of ab-initio molecular polarizabilities. The polarizabilities α_i are then static properties of the atoms, and all changes in the molecular polarizability with respect to the atomic coordinates are due changes in the dipole interaction tensor T_{ij}. However,

the changes in T_{ij} are not large enough to accurately represent the changes in the molecular polarizability with respect to changes in the molecular geometry.

In order to rectify this deficiency in the ADI model, we make the polarizability α_i an explicit function of the size of the atom in a molecule. This approach is inspired by the atoms-in-molecules approach to molecular properties, and by the fact that the polarizability has units of a_0^3. The reasoning is that, as a bond is stretched or compressed, the atom-in-molecule is able to occupy a larger or smaller volume, respectively, assuming that the overlapping charge densities repel each other due to electrostatic effects and Fermi degeneracy. While this is obviously not a correct picture of the electronic structure of a molecule, it employs similar ideas of atomic volume employed in Hirshfeld[25] and Bader partitioning[26] to find atomic charges and polarizabilities.

We define the change in the atomic radius, and thereby the atomic volume, in a given molecule via the overlap of atomic radii. We take the vacuum atomic radius to be the covalent atomic radius. When two atoms (i) and (j) are near each other, we calculate a new radius for atom (i) as:

$$R_i \equiv R_i^{(0)} - 0.5(R_i^{(0)} + R_j^{(0)} - r_{ij}) \tag{7}$$

where $R_i^{(0)}$ is the covalent radius of atom (i), R_i is the new radius, and r_{ij} is the distance between the two atoms. If we define the radius R_j for atom (j) in the same way, then R_i and R_j by definition point towards the other atomic center along a line connecting the two, such that the vectors meet at the plane of intersection of two spheres with radii $R_i^{(0)}$ and $R_j^{(0)}$. This process is illustrated in Figure 1, where we can see that the vectors R_i and R_j result in atomic radii with minimal but nonzero overlap, touching at only a single point between atoms (i) and (j).

We perform the above procedure for every atom in a system, where for atom (i) we define a new radius vector R_i using the nearest neighbor. Note that we define a new radius R_i even if it is greater than the covalent radius $R_i^{(0)}$. In this way we ensure that the volume of each

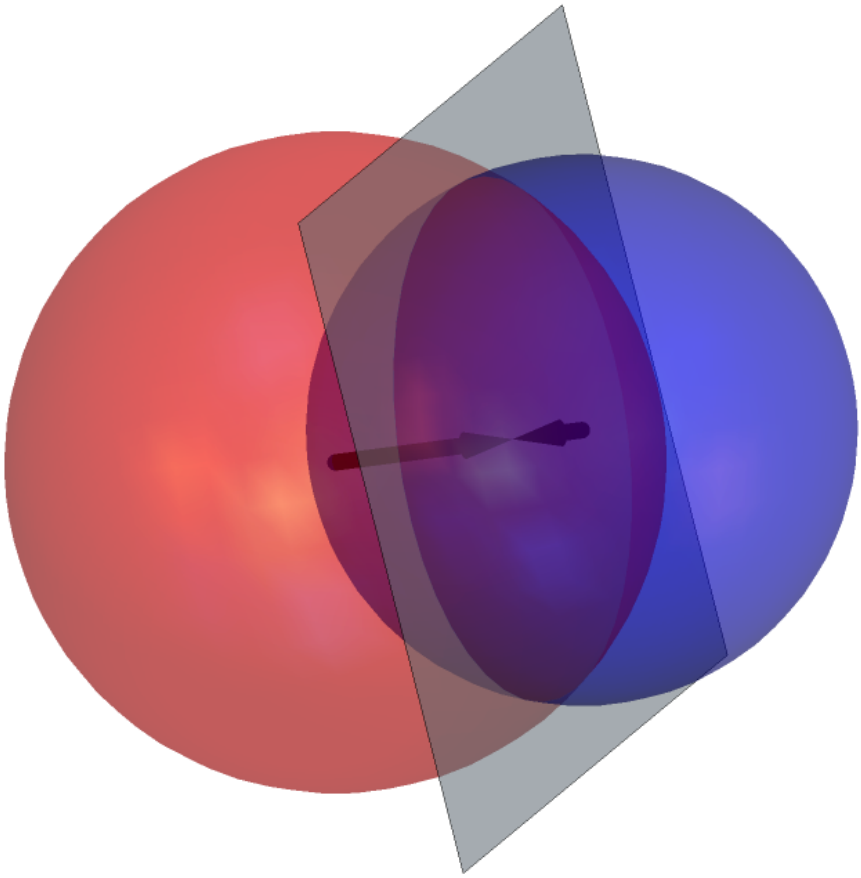

Figure 1: An illustration of the new radii determined by equation 7 for a diatomic molecule. The spheres represent the original, covalent radii, while the spheres formed by the new radii, which have minimal overlap, are not shown. The gray plane shows the intersection between the two spheres and the two arrows show the point at which they meet.

atom in a molecule has a minimal but non-zero overlap with it's nearest neighbor. In other words, the sphere formed by R_i must touch the sphere formed by the nearest neighbor radius R_j at a single point. This effectively means that the volume of an atom in a molecule is determined by its nearest neighbor in the molecule, whether it is expanded or contracted with respect to its vacuum value. Such a procedure is obviously incorrect for a dissociating bond in vacuum, but for systems where no bonds are broken this procedure gives a good measure of the volume occupied by an atom-in-molecule and yields excellent results for the molecular polarizability, as shown below.

Finally, once we have a new radius vector R_i, we can scale the polarizability α_i. Since the polarizability has units of a_0^3, one might assume that it is best to scale α_i by the cube of the ratio of R_i with the covalent radius $R_i^{(0)}$. However, we find that this results in an overestimation of the dependence of the polarizability on the bond length; rather, it is best to scale the polarizability with respect to the ratio $R_i/R_i^{(0)}$. While it's not immediately clear why this is the case, note that we are scaling atom-in-molecule polarizabilities, which we then use to compute the molecular polarizability using the Thole model. The emperically observed linear relationship between polarizability and volume has primarily been observed with molecules, such that all complex interatomic interactions are implicitly included.[27] Thus, in order to better reflect the geometry of the molecule, we scale each diagonal component of the vacuum polarizability α_i by the ratio of the components of the ratio $R_i/R_i^{(0)}$. The scaled polarizability can thus be written:

$$(\alpha_i')_{nn} = (\alpha_i)_{nn} \cdot (R_i/R_i^{(0)})_n \tag{8}$$

Note that by scaling the polarizability by the components of the ratio $R_i/R_i^{(0)}$ we are essentially accounting for the stretching or compressing of a bond between two atoms. We still refer to α_i' as a volume-dependent polarizability though, as α_i' is an atom-centered polarizability which is scaled according to the minimal overlap of spheres centered on neighboring atoms. Once the scaled polarizabilities are obtained, we follow the standard procedure of

ADI methods to find effective polarizabilities, namely using equations 2 and 3 but with α_i' replacing α_i.

When we scale the polarizabilities, a subtle issue arises because the scaling constant in equation 6 is defined by taking the interatomic distance to zero, resulting in a finite interaction energy at zero distance when using static polarizabilities. However, if we scale the polarizabilities using the interatomic distance as in equation 8, the polarizabilities and the scaling constant should go to zero as the interatomic distance goes to zero. While this results in a divergent dipole-dipole interaction, since T_{ij} and α_i^{-1} both scale as R_{ij}^{-1} as the distance $r_{ij} \to 0$, the resulting effective polarizabilities go to zero as $r_{ij} \to 0$. Without a finite dipole-dipole interaction as $r_{ij} \to 0$, one cannot use equation 6 to compute the scaling constant.

Despite this issue, we elect to continue to use equation 6 to define the scaling constant for the "Erf" interaction using the scaled polarizabilities. Our reasoning is that our scaling of the polarizabilities is simply a method to generate polarizability parameters which work for every reasonable configuration of a molecule which we might expect to see in e.g. a molecular dynamics simulation, rather than just the equilibrium configuration. Once these scaled parameters are found for a given molecular configuration, we then freeze the polarizabilities and the fictitious charge densities used to compute the dipole-dipole interactions and let the interatomic distance $r_{ij} \to 0$. We thus recover equation 6 for a large number of configurations of a molecule, but with the scaled polarizabilities. Indeed, in order to obtain equation 6, even without scaling the polarizabilities one must assume the charge density generating the dipole-dipole interaction is unchanged as $r_{ij} \to 0$. Note that this approach is also supported by numerical evidence: we attempted to define the scaling parameter as $R_{ij} = a(\alpha_i^{2/3} + \alpha_j^{2/3})^{1/2}$ where a is a global scaling factor similar to that in equation 4. Fitting the global parameter a to ab-initio data yielded a factor close to that yielded by equation 6. Thus, we believe that our use of equation 6 with the scaled polarizabilities is justified.

The parallel and perpendicularly reduced scattered Raman spectra are calculated using

the following time-dependent formalism:[6]

$$
\begin{aligned}
I_{\parallel}(\omega) &= \frac{\omega}{(\omega-\omega_I)^4}(1-\exp(-\frac{\hbar\omega}{k_BT}))Q(\omega)\int_{-\infty}^{\infty}dte^{-i\omega t}\frac{1}{15}\langle 15\bar{\alpha}(t)\bar{\alpha}(0)+2\mathrm{Tr}[\beta(t)\beta(0)]\rangle \\
I_{\perp}(\omega) &= \frac{\omega}{(\omega-\omega_I)^4}(1-\exp(-\frac{\hbar\omega}{k_BT}))Q(\omega)\int_{-\infty}^{\infty}dte^{-i\omega t}\frac{1}{10}\langle \mathrm{Tr}[\beta(t)\beta(0)]\rangle
\end{aligned}
\tag{9}
$$

where $\bar{\alpha}(t) \equiv (1/3)\mathrm{Tr}[\alpha(t)]$, Tr is the trace, $\beta \equiv \bar{\alpha} - \alpha I$ is the anisotropic part of the polarizability operator, ω_I is the incident radiation frequency, $Q(\omega)$ is a quantum correction factor, and k_B is Boltzmann's constant. Note that the factor of $(\omega-\omega_I)^{-4}$ comes from the definition the reduced Raman spectrum, which ensures that the computed Raman spectrum is directly proportional to the intrinsic Raman scattering activity.[28] The quantum correction factor guarantees the above expressions satisfy the detailed balance condition $I(\omega) = \exp(\hbar\omega/k_BT)I(-\omega)$. We use the harmonic approximation $Q_{HA}(\omega) = \hbar\omega/k_BT/(1-\exp(-\hbar\omega/k_BT))$ as this yields the best results in most cases and obeys the fluctuation dissipation theorem.[29] The expressions for the intensity in this case then become:

$$
\begin{aligned}
I_{\parallel}(\omega) &= (\omega-\omega_I)^{-4}\omega^2\int_{-\infty}^{\infty}dte^{-i\omega t}\frac{1}{15}\langle 15\bar{\alpha}(t)\bar{\alpha}(0)+2\mathrm{Tr}[\beta(t)\beta(0)]\rangle \\
I_{\perp}(\omega) &= (\omega-\omega_I)^{-4}\omega^2\int_{-\infty}^{\infty}dte^{-i\omega t}\frac{1}{10}\langle \mathrm{Tr}[\beta(t)\beta(0)]\rangle
\end{aligned}
\tag{10}
$$

where we have removed constant prefactors for brevity. In order to simplify our calculations, in particular to reduce noise at low frequencies, we use the properties of the time derivative of the Fourier transform to write the intensities in terms of the time derivative of the polarizability:

$$
\begin{aligned}
I_{\parallel}(\omega) &\sim (\omega-\omega_I)^{-4}\int_{-\infty}^{\infty}dte^{-i\omega t}\frac{1}{15}\langle 15\dot{\bar{\alpha}}(t)\dot{\bar{\alpha}}(0)+2\mathrm{Tr}[\dot{\beta}(t)\dot{\beta}(0)]\rangle \\
I_{\perp}(\omega) &\sim (\omega-\omega_I)^{-4}\int_{-\infty}^{\infty}dte^{-i\omega t}\frac{1}{10}\langle \mathrm{Tr}[\dot{\beta}(t)\dot{\beta}(0)]\rangle
\end{aligned}
\tag{11}
$$

Since the polarizabilities in any physically realistic system with a constant number of particles oscillate around an average value, eq. 11 guarantees a signal with zero mean,

thereby guaranteeing the Fourier transform decays to zero at zero frequency. This approach avoids issues with numerical accuracy where small frequencies $\omega \sim 0$ are multiplied by the time average of the correlation functions in eq. 10

Computational Details

All polarizability calculations were performed using the Gaussian16 (rev. A.03)[30] software package. We used the ωB97XD functional[31] with the aug-cc-pVTZ basis set,[32,33] as this combination has been shown to yield accurate polarizabilities for the TABS database.[11] The optimized geometries were taken from the TABS database and were not modified for the polarizability calculations. We optimized the polarizability parameters for the TholeL model using the NLopt library[34] with the "Subplex" algorithm,[35] as it is a highly robust optimization algorithm.

In order to test the TholeL model for non-equilibrium geometries, we generated quasi-random configurations of a small subset of the TABS database. These geometries were generated by running Car-Parinello molecular dynamics (CPMD) simulations of the molecules using the B3LYP[36,37] functional in combination with the cc-pVDZ basis set, as we do not require high accuracy for the resulting geometries. After running each simulation for 0.5 ps with a step size of 0.5 fs, we sampled trajectories every 25 fs and calculated the polarizability for each frame.

In order to test the TholeL model for Raman spectra calculations we ran several simulations of crystalline systems. All trajectories were obtained using the "cp.x" module of Quantum Espresso (v.6.2.1).[38,39] For all simulations we used CPMD with the HSCV pseudoptentials,[40,41] an electron mass of 100 a.u, a timestep of 2.0 a.u. while sampling trajectories every ten steps ($\sim$0.5 fs), and a temperature of 300K. We used the SCAN functional[42] for all simulations except for polyethyelene, where we used the SCAN+rvv10[43] functional, which was necessary to obtain the correct volume of the system at finite temperature. Every simu-

lation was equilibrated using velocity rescaling followed by equilibration with a Nose-Hoover thermostat.[44,45]

We ran the following simulations in order to test the TholeL model for Raman spectroscopy calculations of molecules. We ran an NVE simulation of liquid water using 32 H_2O molecules with a plane-wave cutoff of 90.0 Rydberg for 30 ps. We ran an NVE simulation of a single urea molecule solvated by 32 H_2O molecules with a plane-wave cutoff of 90.0 Rydberg for 30 ps. We ran an NVE simulation of crystalline urea using 16 urea molecules with a plane-wave cutoff of 130.0 Rydberg for 20 ps. Further simulation details are included in the SI.

Results and Discussion

We parameterized the TholeL model and the Thole model, without volume-dependent polarizabilities, on the TABS database using both the "Exp" dipole tensor (eq. 4) and the "Erf" dipole tensor (eq. 5). We chose to parameterize and test our model on the TABS database[22] as it is a reasonably large database, containing 1641 molecules, which features a wide range of common organic molecules up to a reasonably large size (34 atoms). Thorough testing of a small subset of the database has shown that accurate polarizabilities can be obtained using the ωB97XD functional coupled with the aug-cc-pVTZ basis set.[11] We parameterize both models, Thole and TholeL, by reducing the average of the norm of the difference between the ab-initio and approximate polarizabilities:

$$\chi = \frac{1}{N} \sum_i \sqrt{|\alpha_i^{(0)} - \alpha_i|^2} \tag{12}$$

where N is the total number of molecules, $\alpha_i^{(0)}$ is the ab-initio polarizability of the i^{th} molecule, and α_i is the approximate polarizability of the i^{th} molecule. We use a random third of the TABS database to train our model and the remaining two thirds to test the resulting model.

We list the statistics of the error for the optimization of the $\alpha_i^{(0)}$ using the TABS database in Table 1, and we show the correlation between the norms of the exact and approximate polarizabilities in Figure 2. In Table 1 we list the average error as well as the slope (M) and the correlation coefficient (R^2) for the exact and approximate polarizabilities. As we compute the full polarizability tensor for each molecule, we calculate the quantities mentioned above for the norm of the polarizability, the average polarizability, and the anisotropy of the polarizability. The norm is computed as $|\alpha| = \sqrt{\sum_{ij} \alpha_{ij}^2}$, the average is computed as $\langle\alpha\rangle = 1/3 \sum_i \alpha_{ii}$, and the anisotropy is computed as $\delta = 9/2(\langle\alpha^2\rangle - \langle\alpha\rangle^2)$.[46]

Table 1: Statistics of the error of the fit to the TABS database, including the average error and the slope (M) and R^2 coefficient of the correlation between the exact and approximate values. $|\alpha|$, $\langle\alpha\rangle$, and δ refer to the errors for the norm, average polarizability, and anisotropy for the molecules in the TABS database. The "Exp" and "Erf" dipole interactions are defined in the text.

	EXP	EXP-L	ERF	ERF-L
err-$\|\alpha\|$	8.60	10.2	9.82	11.6
err-$\langle\alpha\rangle$	2.76	3.79	3.62	4.59
err-δ	5.40	6.15	5.44	6.26
M-$\|\alpha\|$	0.93	0.92	0.91	0.90
M-$\langle\alpha\rangle$	0.94	0.93	0.92	0.91
M-δ	0.85	0.84	0.92	0.89
R^2-$\|\alpha\|$	0.97	0.96	0.97	0.94
R^2-$\langle\alpha\rangle$	0.98	0.96	0.96	0.94
R^2-δ	0.91	0.88	0.93	0.89

All models yield accurate results for each of the measures chosen. The "Erf" interaction yields significantly more accurate off-diagonal elements as compared to "Exp", as evidenced by the lower error for the anisotropy, but also yields slightly worse average polarizabilities. Note that, while the Thole and TholeL methods yield very similar results, the TholeL model is slightly less accurate. This is mostly due to large molecules which are approximately 1D or 2D, such as anthracene, as the TholeL model tends to underestimate the longitudinal polarizability of the molecule. This is because the TholeL model tends to reduce the effective polarizabilities of atoms in molecules near the ground-state configuration, whereas the effective polarizabilities of the Thole model tend to remain close to their initial values. For

molecules like anthracene, the Thole molecular polarizability is very close to a simple sum over atomic polarizabilities, and so the longitudinal polarizability is quite large and grows approximately linearly with the size of the molecule. For the TholeL model on the other hand, if any atoms have relatively short bonds compared to the rest of the dataset, their effective polarizability can be significantly reduced compared to the initial value, thereby resulting in an underestimation of the longitudinal polarizability. We show this explicitly for 5 molecules in the TABS database with the largest polarizabilities in Tables 2 and 3, which show the average polarizability and anisotropy of the polarizability, respectively, for each molecule and for each model. Note that the TholeL model slightly underestimates the average polarizability and the anisotropy of the polarizability compared to the Thole model.

Table 2: Avg. α (a.u.) of 5 molecules in TABS database with the largest polarizabilities. The "Exp" and "Erf" dipole interactions are defined in the text.

NAME	EXACT	Thole-EXP	TholeL-EXP	Thole-ERF	TholeL-ERF
cinnamaldehyde	122	92	86	100	95
E(1,3,5)hexatriene	94	64	61	73	69
azulene	130	94	89	102	98
heptalene	153	113	103	125	121
phenazine	169	123	117	136	132
anthracene	179	129	121	141	135

Table 3: Anisotropy of α (a.u.) of 5 molecules in TABS database with the largest polarizabilities. The "Exp" and "Erf" dipole interactions are defined in the text.

NAME	EXACT	Thole-EXP	TholeL-EXP	Thole-ERF	TholeL-ERF
cinnamaldehyde	115	21	12	93	81
E(1,3,5)hexatriene	102	13	8	75	62
azulene	109	21	13	91	84
heptalene	112	22	19	88	84
phenazine	169	32	21	138	127
anthracene	172	34	24	138	125

We further test the generality of the Thole and TholeL models by comparing their performance for non-equilibrium geometries of molecules. For a small subset of molecules in the TABS database(SI), we run CPMD simulations of each molecule to generate a series of ran-

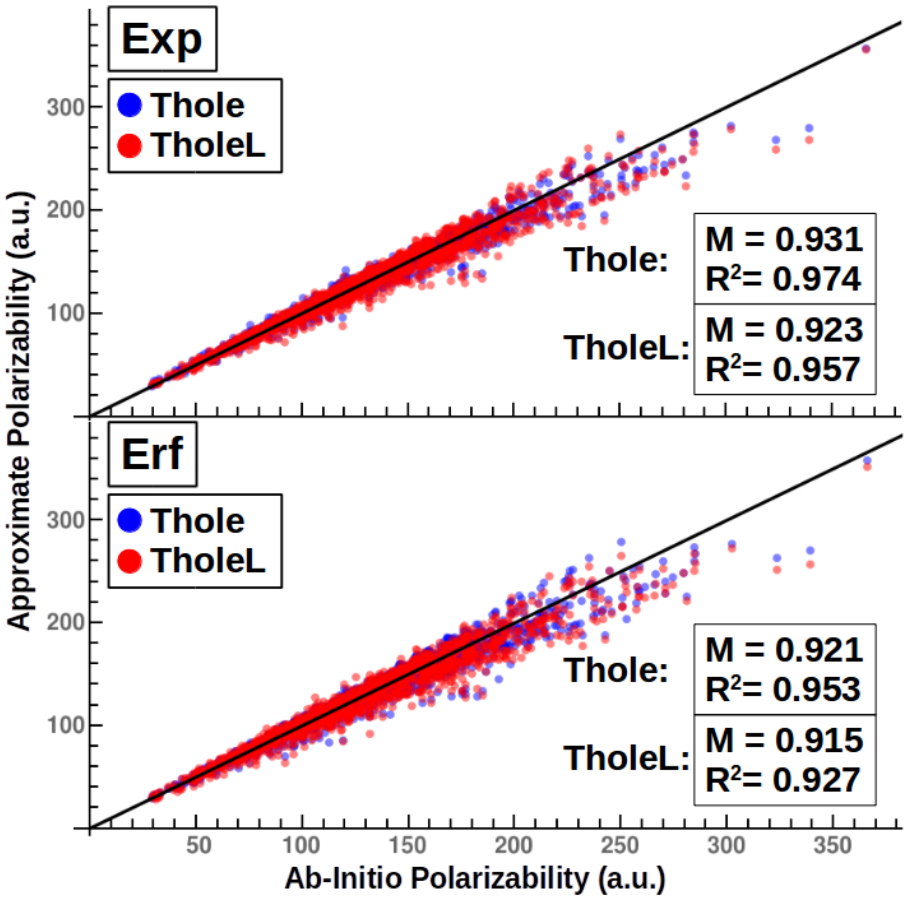

Figure 2: Correlation plots of the norms of the ab-initio and approximate polarizabilities of the TABS database for the Thole and TholeL models for both the "Exp" and "Erf" interactions. The blue points show results from the Thole model while the red points show results from the TholeL model.

dom perturbations to the ground-state geometry, with an average standard deviation of the polarizability $\sim$3 bohr^3 for each molecular configuration. We then calculate approximate polarizabilities of these geometries using parameters obtained from training to the entire TABS database. The correlation plots (Figure 3) show that the TholeL model significantly outperforms the Thole model. Note in particular that, although the Thole polarizabilities roughly follow a line of unit slope overall, the plot is composed of a series of overlapping horizontal lines. This indicates that, while the Thole model yields accurate average polarizabilities for each molecule, it does not in general yield quantitatively accurate derivatives of the polarizability with respect to atomic positions. On the other hand, the TholeL data is composed of a series of overlapping diagonal lines, indicating that the TholeL model yields accurate average polarizabilities and polarizability derivatives for each molecule. We can make this analysis more formal by looking at the mean slope and R^2 for each correlation plot for each molecule, which we list in Table 4. While there are still inaccuracies in the TholeL model, Table 4 shows that it greatly improves the polarizability derivatives over the Thole model.

Table 4: Average M and R^2 for the polarizabilities of each set of configurations for each molecule in the subset of the TABS database for which we generated random configurations, where the "Erf" and "Exp" dipole interactions are defined in the text.

Model	$\langle M \rangle$	$\langle R^2 \rangle$
Thole-Exp	0.117	0.362
TholeL-Exp	0.417	0.569
Thole-Erf	0.286	0.712
TholeL-Erf	0.586	0.745

In order to compare the performance of the two models with respect to molecular configuration in more detail, we consider two specific examples. The first example is H_2O, as it is such an important molecule, and accurate models of its polarizability can significantly improve statistical quantities in MD simulations.[3] We plot the polarizability of H_2O predicted by the Thole and TholeL models with respect to the ab-initio polarizability in Figure 4, where each r(OH) distance is set to 0.9575 Å and is varied within [-0.3Å,0.2Å] with a step

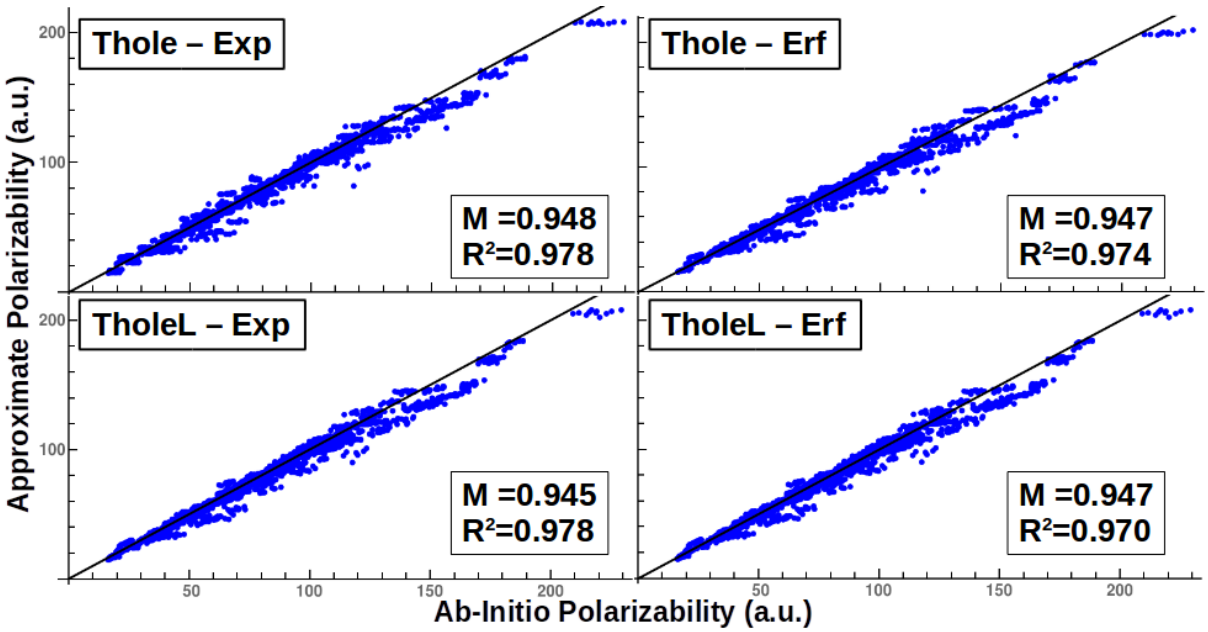

Figure 3: Correlation plots of the norms of the ab-initio and approximate polarizabilities of random perturbations of a subset of molecules in the TABS database. Each panel shows the results using either the Thole or TholeL model with either the "Exp" or "Erf" dipole interaction, as defined in the text.

of 0.025 Å and the θ(HOH) angle is set to 104.5° and is varied within $[-40^\circ, 40^\circ]$ with a step of 5°. Figure 4 shows that the Thole model can at times yield quantitatively accurate polarizability derivatives near the equilibrium configuration. However, in most cases, the Thole model yields neither quantitatively accurate polarizabilities nor derivatives of the polarizability with respect to internal atomic coordinates, as is the case with the H_2O molecule and the "Exp" dipole interaction. The TholeL model on the other hand, improves the polarizabilities yielded by the "Exp" interaction for all molecular configurations and yields accurate polarizabilities with the "Erf" interaction over essentially the entire range of sampled geometries. Thus, paired with the proper dipole interaction, the TholeL model can yield quantitatively accurate molecular polarizabilities for essentially all reasonable configurations likely to be found in molecular dynamics simulations.

To further illustrate the performance of the TholeL model we consider a second example: a dissociating H_2 molecule. In this case, we used CCSD(T) with the dAug-cc-pVTZ basis to both optimize the H_2 geometry and calculate the polarizability. We set the r(HH) distance

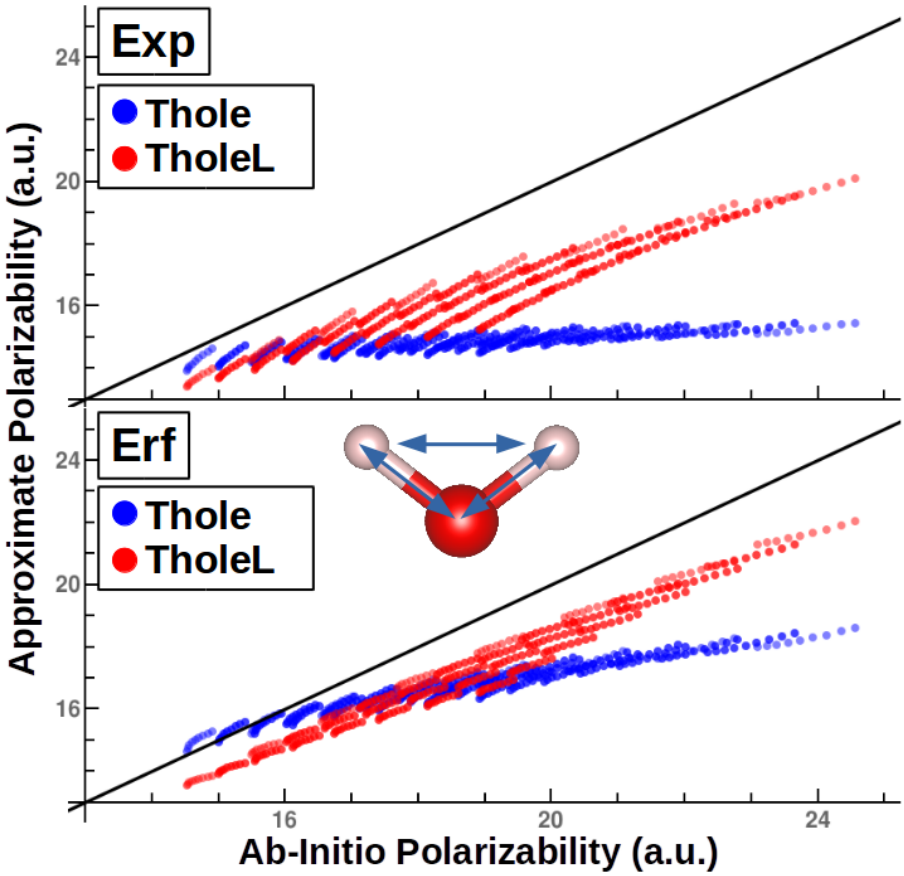

Figure 4: The polarizability of H_2O with respect to molecular configuration. The blue points are those obtained using the Thole model while the red points are those obtained using the TholeL model.

to the ground state value of 0.7431 Å and then sample the polarizability at distances from [-0.2Å,2.2Å] with respect to the ground state. We plot the longitudinal, perpendicular and average polarizability of H_2 obtained from CCSD(T), Thole, and TholeL in Figure 5. Once again, the Thole model is qualitatively correct, reproducing the overall trends while failing to yield accurate polarizabilities far from the ground state. The TholeL model tends to overestimate changes in the longitudinal polarizability and underestimate changes in the perpendicular polarizability, but still yields excellent results for both components and the average polarizability all the way up to the dissociation point at ∼3.1 Å, especially for the "Erf" interaction. Past the point of dissociation, the TholeL model is no longer accurate as the dependence on the interatomic distance is determined only by the nearest-neighbor distance, without any regard to bond breaking. This was to simplify the model and reduce the number of parameters by not making reference to bond length parameters, as the intended use of the TholeL model is condensed systems. Yet, in Figure 5 we see that even for rather extreme bond fluctuations the TholeL model still yields accurate results.

Since the TholeL model with the "Erf" dipole interaction yields accurate derivatives of the molecular polarizability with respect to atomic positions, the TholeL model should yield accurate Raman spectra for a wide range of systems. To test this hypothesis, we calculated Raman spectra from CPMD trajectories using the SCAN functional and the "Erf" dipole interaction for several different systems where the Raman spectrum is an important tool for characterization.

We first calculate the Raman spectrum $I_{||}(\omega)$ and $I_{\perp}(\omega)$ for liquid water at 300 K from a simulation of 32 H_2O molecules in figures 6 and figure 7, where we see the TholeL model yields excellent agreement with experiment.[28] While the frequencies of the different peaks are determined from the underlying forces associated with the functional, the intensity and shape of the resulting peaks is entirely a result of the form and parameters of the TholeL model. The ratio of the intensities remarkably close to what is observed in experiment: the O-H stretching mode (∼3400 cm^{-1}) should be ∼100x larger than the bending mode

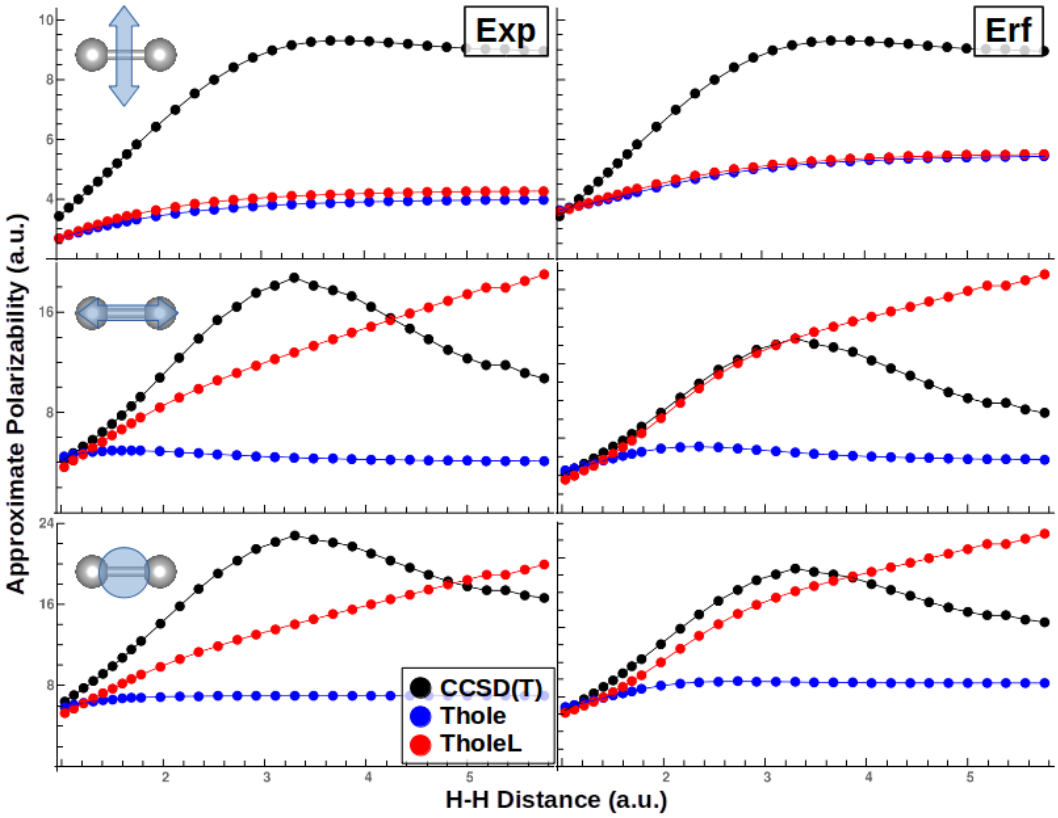

Figure 5: The polarizability of the H_2 molecule with respect to the H-H distance. The black points are calculated using CCSD(T), blue points using the Thole model, and red points using the TholeL model.

(∼1700 cm^{-1}), though the librational band (∼600 cm^{-1}) is slightly too large compared to the bending mode. However, we note the agreement is excellent given the simplicity of the model we are using and is comparable to results from much more sophisticated models, e.g. MB-pol.[47] Importantly, the Raman intensities are dramatically improved with respect to the Thole model, which underestimates the amplitude in the O-H stretching region by over an order of magnitude.

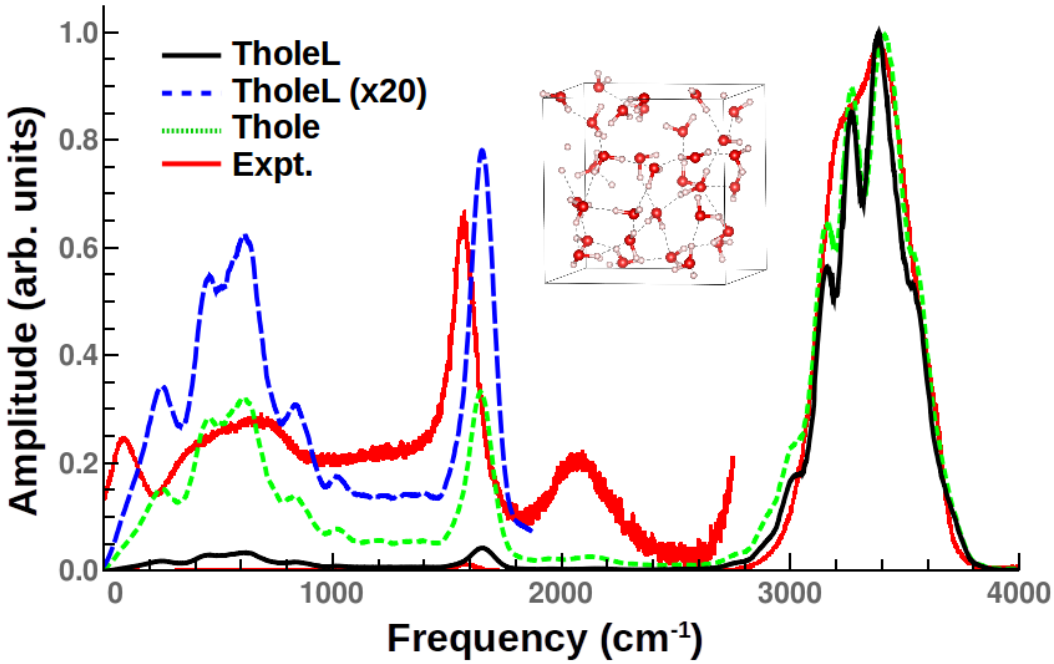

Figure 6: The Raman spectrum, $I_{\parallel}(\omega)$,of water calculated from the Thole and TholeL models (normalized to unity). The black solid line is the spectrum normalized to unity, while the blue dashed line is the same multiplied by 20, and the green dotted line is the Thole spectrum. The red points show the experimental spectrum.[28]

In order to demonstrate the generality of the TholeL model, we calculate the Raman spectrum of urea in different bonding environments. We choose to study the urea molecule as it is a well-studied test case in polarizability calculations,[18,48] and Raman spectra have been reported in a number of environments.[49–51] We plot the Raman spectrum for crystalline urea in Figure 8, with the N-H stretching region shown in Figure 8a and the C-H stretching and NH_2 bending regions shown in Figure 8b. The Thole and TholeL spectra in the N-H stretching region are quite similar, but at lower frequencies in Figure 8b we see significant

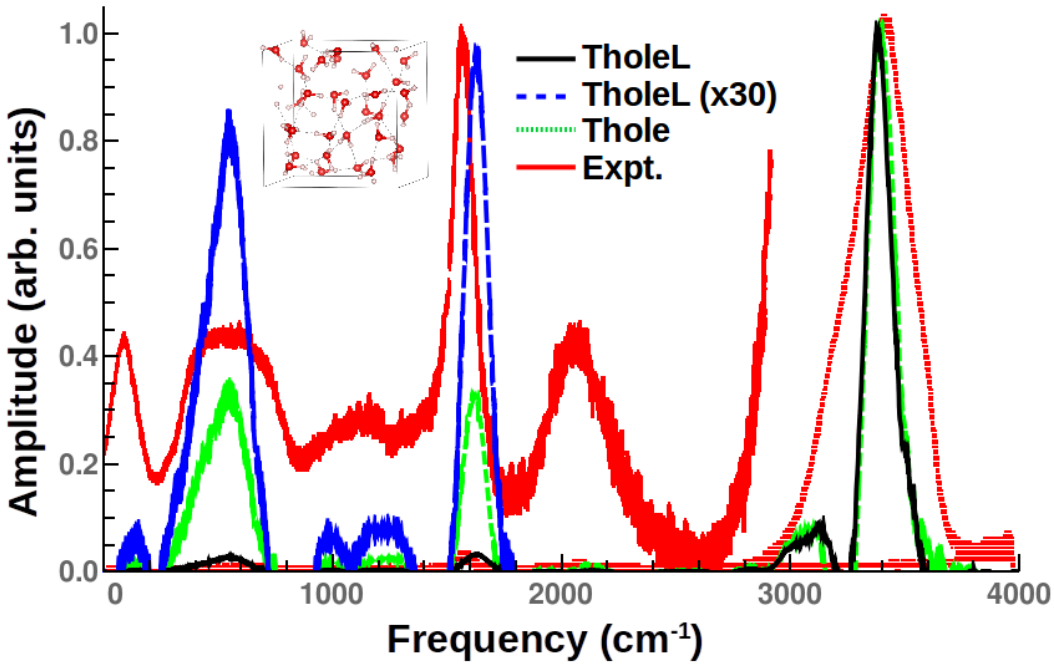

Figure 7: The Raman spectrum, $I_{\perp}(\omega)$,of water calculated from the Thole and TholeL models (normalized to unity). The black solid line is the spectrum normalized to unity, while the blue dashed line is the same multiplied by 30, and the green dotted line is the Thole spectrum. The red points show the experimental spectrum.[28]

differences between the two models. We have labelled the peaks according to the molecular motions as either bending (b), stretching (s), rocking (r), or symmetric stretching (ss). Experiments show the NCN(ss) peak should be roughly 10 times that of the NH_2(b) and CO(s) peaks, which themselves should be roughly equal in amplitude.[52] While the TholeL model yields intensities which roughly match experiments, the Thole model vastly underestimates the amplitutde of the NCN(ss) peak while overestimating the amplitude of the CO(s) peak.

In addition to crystalline urea, we also computed Raman spectra for a urea molecule solvated by 32 H_2O molecules. In order to investigate the impact of solvation on the Raman spectrum, we compute effective polarizabilities for all atoms in the system, but we plot the Raman spectra for only urea for the Thole and TholeL models in Figure 9. Once again, the bending region in Figure 9b, we see that the Thole model underestimates the amplitude of the NCN stretching peak at $\sim$1000 cm^{-1} compared to the NH_2 bending peak at $\sim$1175 cm^{-1}. Experiments predict the C-N stretching peak should be roughly 10 times larger than the NH_2

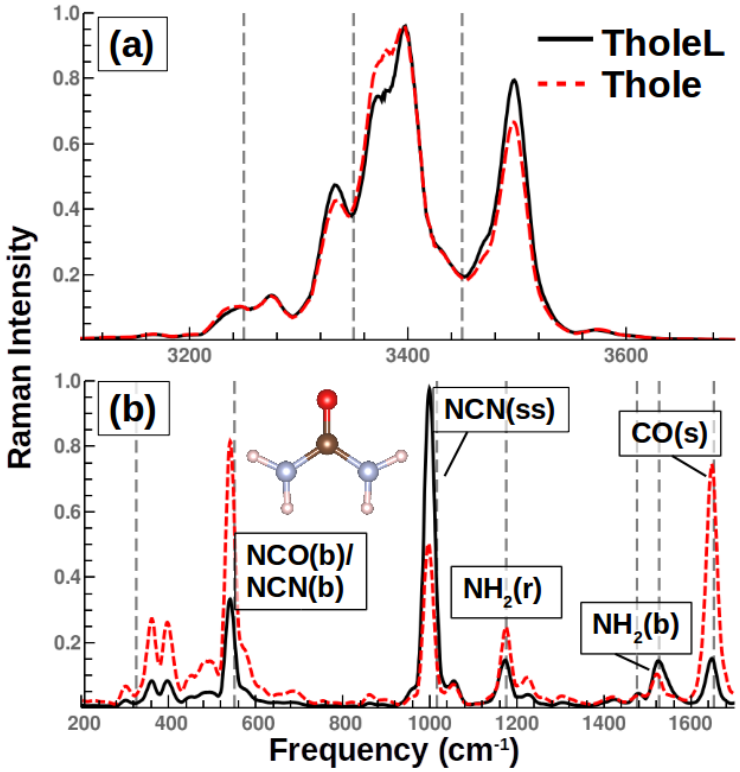

Figure 8: The calculated Raman spectrum $I_{\|}(\omega)$ of crystalline urea, where the solid black line and dashed red line show the TholeL and Thole spectra, respectively. The dashed vertical lines show the observed peak values.[52] All spectra have been normalized to fit on the same plot. The three panels each show a different frequency range.

rocking peak,[50,53] the TholeL model predicts a ratio of 6, while the Thole model predicts a ratio of 1.5. Figure 9a also shows that the Thole model predicts a strong CO(s) and NH_2(b) peak around 1500-1600 cm^{-1}, while both the TholeL model and experiments show that these modes only contribute a broad, low band, consistent with experiments.[53] Thus, the TholeL model yields significant improvements for urea solvated by water in addition to crystalline urea.

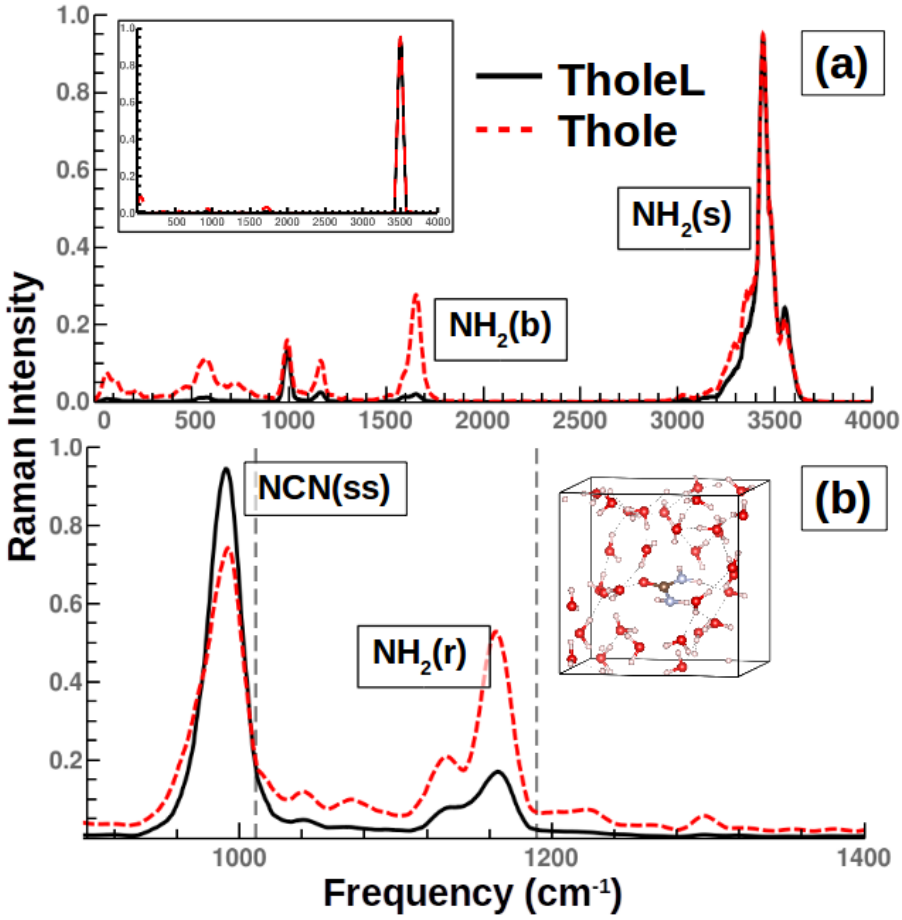

Figure 9: The calculated Raman spectrum $I_{\|}(\omega)$ of urea solvated by 32 H_2O molecules, where the solid black line and dashed red line show the TholeL and Thole spectra, respectively. The dashed vertical lines show the experimentally observed peak values of urea in water.[50,53] All spectra have been normalized to fit on the same plot.

Conclusion

In conclusion, we have introduced a new model for the polarizability based on the Thole model and volume-dependent atomic polarizabilities. Without adding any new parameters to the model, but simply considering the volume occupied by an atom-in-molecule and scaling the atomic polarizability by the ratio of the radius of the spherical volume to the covalent radius, we have significantly improved the generality of the Thole model. While this model violates the empirical rule that the polarizability is linearly related to the volume,[27] note that we are scaling the atom-in-molecule polarizabilities, while the empirical linear relationship has been tested primarily with molecular polarizabilities and volumes. Our approach to the "atomic volume" is a relatively simple idea that nonetheless yields excellent results for a wide range of molecules in a diverse array of configurations and condensed phase environments. By further expanding our ideas on the atomic volume in a molecule and how it impacts the polarizability and possibly other properties, even greater improvements in accuracy and generality may be possible. Even with the simple model we have introduced however, we are able to use the TholeL model to calculate highly accurate Raman spectra from ab-initio trajectories for a diverse array of materials. With the accuracy of the TholeL model over a wide range of molecular configurations, this model might also be useful for molecular simulations, where accurate polarizabilities are required for all possible configurations of a molecule in a given ensemble.

Acknowledgement

This work was supported by the Center for Complex Materials, an Energy Frontier Research Center funded by the US Department of Energy, Office of Science, Basic Energy Sciences under Grant No. DE-SC0012575 and by the US Army Research Laboratory under Contract No. W911NF-16-2-0189. This research includes calculations carried out on Temple University's HPC resources and thus was supported in part by the National Science Foun-

dation through major research instrumentation grant number 1625061 and by the US Army Research Laboratory under contract number W911NF-16-2-0189.

Supporting Information Available

The supplemental information contains the set of molecules used to generate random configurations with CPMD, the simulation details for the CPMD simulations used to compute Raman spectra, and the optimized polarizability parameters used in all polarizability calculations.

References

(1) Brooks, B. R.; Bruccoleri, R. E.; Olafson, B. D.; States, D. J.; Swaminathan, S.; Karplus, M. CHARMM: A Program for Macromolecular Energy, Minimization, and Dynamics Calculations. *Journal of Computational Chemistry* **1983**, *4*, 187–217.

(2) Lamoureux, G.; MacKerell, A. D.; Roux, B. A Simple Polarizable Model of Water Based on classical Drude oscillators. *The Journal of Chemical Physics* **2003**, *119*, 5185–5197.

(3) Chialvo, A. A.; Cummings, P. T. Simple Transferable Intermolecular Potential for the Molecular Simulation of Water Over Wide Ranges of State Conditions. *Fluid Phase Equilibria* **1998**, *150-151*, 73–81.

(4) Warshel, A.; Kato, M.; Pisliakov, A. V. Polarizable Force Fields: History, Test Cases, and Prospects. *Journal of Chemical Theory and Computation* **2007**, *3*, 2034–2045.

(5) Thompson, M. A. QM/MMpol: A Consistent Model for Solute/Solvent Polarization. Application to the Aqueous Solvation and Spectroscopy of Formaldehyde, Acetaldehyde, and Acetone. *The Journal of Physical Chemistry* **1996**, *100*, 14492–14507.

(6) McQuarrie, D. A. *Statistical Mechanics*; University Science Books: Sausalito, CA, 2000.

(7) Boyd, R. *Nonlinear Optics*; Elsevier, 2008.

(8) Shen, Y. R. *The Principles of Nolinear Optics*; Wiley, 2003.

(9) Hickey, A. L.; Rowley, C. N. Benchmarking Quantum Chemical Methods for the Calculation of Molecular Dipole Moments and Polarizabilities. *The Journal of Physical Chemistry A* **2014**, *118*, 3678–3687.

(10) Christiansen, O.; Halkier, A.; Koch, H.; Jørgensen, P.; Helgaker, T. Integral-Direct Coupled Cluster Calculations of Frequency-Dependent Polarizabilities, Transition Probabilities and Excited-State Properties. *The Journal of Chemical Physics* **1998**, *108*, 2801–2816.

(11) Wu, T.; Kalugina, Y. N.; Thakkar, A. J. Choosing a Density Functional for Static Molecular Polarizabilities. *Chemical Physics Letters* **2015**, *635*, 257–261.

(12) Kang, Y. K.; Jhon, M. S. Additivity of Atomic Static Polarizabilities and Dispersion Coefficients. *Theoretica chimica acta* **1982**, *61*, 41–48.

(13) Zhou, T.; Dykstra, C. E. Additivity and Transferability of Atomic Contributions to Molecular Second Dipole Hyperpolarizabilities. *The Journal of Physical Chemistry A* **2000**, *104*, 2204–2210.

(14) Silberstein, L. VII. Molecular Refractivity and Atomic Interaction. *The London, Edinburgh, and Dublin Philosophical Magazine and Journal of Science* **1917**, *33*, 92–128.

(15) Applequist, J.; Carl, J. R.; Fung, K.-K. Atom Dipole Interaction Model for Molecular Polarizability. Application to Polyatomic Molecules and Determination of Atom Polarizabilities. *Journal of the American Chemical Society* **1972**, *94*, 2952–2960.

(16) Thole, B. Molecular Polarizabilities Calculated with a Modified Dipole Interaction. *Chemical Physics* **1981**, *59*, 341–350.

(17) Wang, J.; Cieplak, P.; Li, J.; Hou, T.; Luo, R.; Duan, Y. Development of Polarizable Models for Molecular Mechanical Calculations I: Parameterization of Atomic Polarizability. *The Journal of Physical Chemistry B* **2011**, *115*, 3091–3099.

(18) Jensen, L.; Sylvester-Hvid, K. O.; Mikkelsen, K. V.; Åstrand, P.-O. A Dipole Interaction Model for the Molecular Second Hyperpolarizability. *The Journal of Physical Chemistry A* **2003**, *107*, 2270–2276.

(19) Jensen, L.; Åstrand, P.-O.; Sylvester-Hvid, K. O.; Mikkelsen, K. V. Frequency-Dependent Molecular Polarizability Calculated within an Interaction Model. *The Journal of Physical Chemistry A* **2000**, *104*, 1563–1569.

(20) Birge, R. R. Calculation of Molecular Polarizabilities Using an Anisotropic Atom Point Dipole Interaction Model which Includes the Effect of Electron Repulsion. *The Journal of Chemical Physics* **1980**, *72*, 5312.

(21) DelloStritto, M.; Piontek, S. M.; Klein, M. L.; Borguet, E. Relating Interfacial Order to Sum Frequency Generation with Ab Initio Simulations of the Aqueous $Al_2O_3(0001)$ and $(11\bar{2}0)$ Interfaces. *The Journal of Physical Chemistry C* **2018**, *122*, 21284–21294.

(22) Blair, S. A.; Thakkar, A. J. TABS: A Database of Molecular Structures. *Computational and Theoretical Chemistry* **2014**, *1043*, 13–16.

(23) Jensen, L. L.; Jensen, L. Electrostatic Interaction Model for the Calculation of the Polarizability of Large Noble Metal Nanoclusters. *The Journal of Physical Chemistry C* **2008**, *112*, 15697–15703.

(24) Mayer, A. Formulation in Terms of Normalized Propagators of a Charge-Dipole Model Enabling the Calculation of the Polarization Properties of Fullerenes and Carbon Nanotubes. *Physical Review B* **2007**, *75*, 045407.

(25) Hirshfeld, F. L. Bonded-Atom Fragments for Describing Molecular Charge Densities. *Theoretica chimica acta* **1977**, *44*, 129–138.

(26) Bader, R. F. W.; Henneker, W. H.; Cade, P. E. Molecular Charge Distributions and Chemical Binding. *The Journal of Chemical Physics* **1967**, *46*, 3341–3363.

(27) Brinck, T.; Murray, J. S.; Politzer, P. Polarizability and Volume. *The Journal of chemical physics* **1993**, *98*, 4305–4306.

(28) Brooker, M. H.; Hancock, G.; Rice, B. C.; Shapter, J. Raman Frequency and Intensity Studies of Liquid H_2O, $H_2{}^{18}O$ and D_2O. *Journal of Raman Spectroscopy* **1989**, *20*, 683–694.

(29) Ramìrez, R.; Lòpez-Ciudad, T.; Kumar P, P.; Marx, D. Quantum Corrections to Classical Time-Correlation Functions: Hydrogen Bonding and Anharmonic Floppy Modes. *The Journal of Chemical Physics* **2004**, *121*, 3973–3983.

(30) Frisch, M. et al. Gaussian16 A.03. 2016; `http://gaussian.com/`, Gaussian Inc., Wallingford, CT.

(31) Chai, J.-D.; Head-Gordon, M. Long-Range Corrected Hybrid Density Functionals with Damped Atom-Atom Dispersion Corrections. *Physical Chemistry Chemical Physics* **2008**, *10*, 6615–6620.

(32) Kendall, R. A.; Dunning, T. H., Jr.; Harrison, R. J. Electron Affinities of the First-Row Atoms Revisited. Systematic Basis Sets and Wave Functions. *The Journal of Chemical Physics* **1992**, *96*, 6796–6806.

(33) Dunning, T. H. Gaussian Basis Sets for Use in Correlated Molecular Calculations. I. The Atoms Boron Through Neon and Hydrogen. *The Journal of Chemical Physics* **1989**, *90*, 1007–1023.

(34) Johnson, S. G. The NLopt Nonlinear-Optimization Package. `http://ab-initio.mit.edu/nlopt`.

(35) Rowan, T. Functional Stability Analysis of Numerical Algorithms. Ph.D Thesis, University of Texas at Austin, Austin, Texas, 1990.

(36) Becke, A. D. Density-Functional Exchange-Energy Approximation with Correct Asymptotic Behavior. *Physical Review A* **1988**, *38*, 3098–3100.

(37) Lee, C.; Yang, W.; Parr, R. G. Development of the Colle-Salvetti Correlation-Energy Formula into a Functional of the Electron Density. *Physical Review B* **1988**, *37*, 785–789.

(38) Giannozzi, P. et al. QUANTUM ESPRESSO: a Modular and Open-Source Software Project for Quantum Simulations of Materials. *Journal of Physics: Condensed Matter* **2009**, *21*, 395502.

(39) Giannozzi, P. et al. Advanced Capabilities for Materials Modelling with Quantum ESPRESSO. *Journal of Physics: Condensed Matter* **2017**, *29*, 465901.

(40) Hamann, D. R.; Schlüter, M.; Chiang, C. Norm-Conserving Pseudopotentials. *Physical Review Letters* **1979**, *43*, 1494–1497.

(41) Vanderbilt, D. Optimally Smooth Norm-Conserving Pseudopotentials. *Physical Review B* **1985**, *32*, 8412–8415.

(42) Sun, J.; Ruzsinszky, A.; Perdew, J. Strongly Constrained and Appropriately Normed Semilocal Density Functional. *Physical Review Letters* **2015**, *115*, 036402.

(43) Sabatini, R.; Gorni, T.; de Gironcoli, S. Nonlocal van der Waals Density Functional Made Simple and Efficient. *Physical Review B* **2013**, *87*, 041108.

(44) Nos, S. A Unified Formulation of the Constant Temperature Molecular Dynamics Methods. *The Journal of Chemical Physics* **1984**, *81*, 511–519.

(45) Bylander, D. M.; Kleinman, L. Energy Fluctuations Induced by the Nosé Thermostat. *Physical Review B* **1992**, *46*, 13756–13761.

(46) Applequist, J. Atom Charge Transfer in Molecular Polarizabilities: Application of the Olson-Sundberg Model to Aliphatic and Aromatic Hydrocarbons. *The Journal of Physical Chemistry* **1993**, *97*, 6016–6023.

(47) Medders, G. R.; Paesani, F. Infrared and Raman Spectroscopy of Liquid Water through "First-Principles" Many-Body Molecular Dynamics. *Journal of Chemical Theory and Computation* **2015**, *11*, 1145–1154.

(48) Pluta, T.; Sadlej, A. J. Electric Properties of Urea and Thiourea. *The Journal of Chemical Physics* **2001**, *114*, 136–146.

(49) Keuleers, R.; Desseyn, H. O.; Rousseau, B.; Van Alsenoy, C. Vibrational Analysis of Urea. *The Journal of Physical Chemistry A* **1999**, *103*, 4621–4630.

(50) Hoccart, X.; Turrell, G. Raman Spectroscopic Investigation of the Dynamics of Urea-Water Complexes. *The Journal of Chemical Physics* **1993**, *99*, 8498–8503.

(51) Langer, J.; Schrader, B.; Bastian, V.; Jacob, E. Infrared Spectra and Force Constants of Urea in the Gaseous Phase. *Fresenius' Journal of Analytical Chemistry* **1995**, *352*, 489–495.

(52) Frost, R. L.; Kristof, J.; Rintoul, L.; Kloprogge, J. T. Raman Spectroscopy of Urea and Urea-Intercalated Kaolinites at 77 K. *Spectrochimica Acta Part A: Molecular and Biomolecular Spectroscopy* **2000**, *56*, 1681–1691.

(53) Wen, N.; Brooker, M. H. Urea protonation: Raman and Theoretical Study. *The Journal of Physical Chemistry* **1993**, *97*, 8608–8616.

Graphical TOC Entry

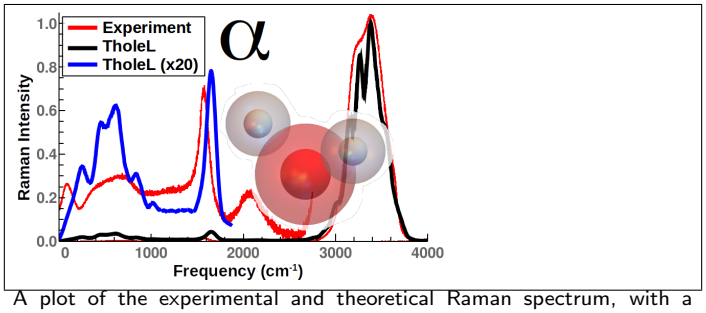

A plot of the experimental and theoretical Raman spectrum, with a graphic illustrating the volume-dependence of the polarizability.